Frequency domain response of a propfan using finite element method and experimental study on a rotor

Luís Guilherme Figueira Franco
guilherme.franco@tecnico.ulisboa.pt

Instituto Superior Técnico, Universidade de Lisboa, Portugal
November 2017

ABSTRACT

Nowadays, the study of Rotordynamics is fundamental to understand the behaviour of most rotating machinery, such as: turbines; compressors; pumps and generators. In the aeronautical industry, the Rotordynamics field is very important and mostly used in the subject of aircraft engines. Since it is inevitable to avoid faults in real structures, due to imperfect manufacturing or unwanted operation accidents, it is essential to design, predict and correct the behaviour of rotating machinery.

In this context, this article focuses on the main theme of this thesis, i.e., the validation of the numerical method (Finite Element Method, FEM) of the dynamic response of rotor machinery through a direct comparison of the results obtained with other numerical, analytical and experimental models. After mounting the experimental setup, one can compare the natural frequencies and critical velocities obtained experimentally with the results from the analytical and numerical models, thus validating the numerical model (FEM) used in this work. After concluding the validation process, the proposed numerical method is applied to a case study of aeronautics, the Propfan engine created by the European project DUPRIN.

Keywords: Rotordynamics; Frequency domain; Finite Element Method; Experimental Modal Analysis; Propfan.

1. INTRODUCTION

The large increase in rotational speed of many machinery components made it critical to include rotation into the analysis of their dynamic behaviour. Most of rotordynamics studies were motivated by turbomachines being incapable of producing their estimated performance or even functioning at all due to the lack of some rotordynamics requirements. Obtaining the frequency response curves from rotor systems is a problem of high importance to understand their vibrational response. The contribution of this analysis is quite noticeable, since it will allow fundamental statements on vibrational behaviour of rotor machinery and their elements, discovering excitations, their causes and defining critical or dangerous rotational speeds creating the required precautions to avoid possible risks.

Considering the evolution of new and more complex rotor systems, new solving methods were developed and applied to rotordynamics, such as the FEM. The first rotordynamics finite element model was first introduced by Ruhl and Booker [1], which included elastic bending energy and translational kinetic energy. Subsequently, Nelson and McVaugh [2] developed a finite element model for both stationary and rotating reference, which included the gyroscopic moment
and axial loading. Later, Nelson [3] and Genta [4] applied the Timoshenko beam theory to rotor systems.

Lalanne and Ferraris [5] also present essential numerical methods for rotordynamics. Their work includes the description of the basic rotor components, the derivation of the basic equations of motion and the application of the FEM to some industrial results, such as the Propfan engine. Genta [6] and Rao [7] also introduce an accurate explanation on rotordynamics field, including nonlinear and nonstationary phenomena, asymmetric rotor geometries, various fault models (misalignment, unbalanced, bent shafts) and 3D modelling. One should also mention the recent MSC thesis of Rafael Carvalho [8] and Miguel Matos [9], who in their respective works created models for a finite element analysis in order to study the lateral dynamic behaviour of rotors and used force identifications methods applied to rotordynamics, since one of this project's main objective is the complementation of their initial work.

Relatively to experimental modal analysis, one may highlight the work developed by Silva [10], who refers to the concentrated mass method used to analyse continuous structures characterized into spacial mass elements, stiffness and damping. This method is part of the base development of the experimental modal analysis, which allows the determination of the dynamic properties of a structure through its frequency response functions (FRFs). In [11] Maia and Silva also presents an extensive work in this subject, where it presents the methodology to develop a Modal Model and a Response Model from the Spatial Model, and how they relate with one another through the FRFs and modal properties, such as natural frequencies, mode shapes and modal damping. The document presented by Schwarz and Richardson [12] also contains some concepts related to experimental modal analysis, mainly focused on the verification and validation of models.

This article is composed by three sections; the first introduces some fundamentals and theory of rotordynamics, including a mathematical model used to represent the rotor system elements based on their energy equations and the deduction of the rotor's equation of motion. Furthermore, it is also included the different numerical and experimental methodologies adopted in this work. One also presents a brief introduction of two numerical models (steel beam and a mono-rotor), created in *ANSYS* environment. Then, in the experimental methodology, one indicates some aspects related to the experimental models and the procedure applied to each test.

2. FUNDAMENTALS

2.1. Rotordynamics Fundamentals

The field of engineering that studies the lateral and torsional vibrations of rotating shafts is called rotordynamics. One of its objectives is the prediction of excessive vibrations applied on the rotor ensuring the safe and reliable operation of rotating structures. Some aspects like gyroscopic moments, cross-coupled forces, critical speeds and whirling effects are investigated in rotordynamics and are not studied in structural vibration analysis. Rotor systems can be simplified into several elementary parts, which include the disk, the shaft and bearings. Also, loads are usually caused by mass unbalances that cannot be avoided. Nonetheless, loads applied on the rotor may have origin associated to unbalanced rotors (synchronous excitation), bearing asymmetry (asynchronous excitation) and harmonic forces.

One simple rotor configuration consists of a supported rotating beam with an accompanying disk. This type of systems are known as monorotor or Jeffcott rotor [13], which is displayed in Figure 1. Lalanne and Ferraris [5] provides a revision on the dynamics of such rotors and includes a deduction of a finite element model to study this type of structures.

The rotor of Figure 1 is composed by a flexible shaft of length L with a single rigid disk located at $Y = l_1$ and a discrete bearing at $Y = l_2$. The model is assumed to be simply supported at both ends and the bearing characteristics, i.e. stiffness and damping coefficients, indicate if the rotor is symmetric or asymmetric.

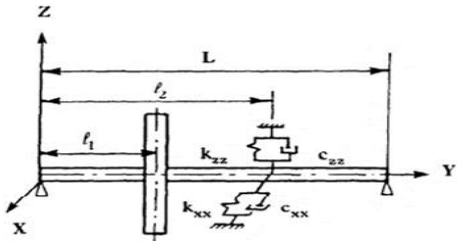

Figure 1 – Lalanne and Ferraris theoretical model of the mono-rotor (source [5]).

The shaft is modelled as a flexible beam with circular cross-section resorting to the Euler-Bernoulli beam theory with transverse shear correction. It is composed by an isotropic, homogeneous material with no internal damping and following a linear behaviour. The element matrices of this element include the effects of rotatory inertia, gyroscopic moments, shear deformation and axial load. However, axial torque and internal damping are not considered. The disk is considered axis-symmetric and modelled as a rigid body, which is characterized by its mass and inertial properties. Lastly, the bearings are modelled as a linear spring-damper element in the $X - Z$ plane.

To obtain the equation of motion, the rotor is described into several elements characterized by a total of n degrees of freedom. Subsequently, the governing equations are combined with these quantities to obtain the equations that characterize the linearized structure behaviour:

$$[M]\{\ddot{q}(t)\} + [C]\{\dot{q}(t)\} + [K]\{q(t)\} = \{f(t)\} \tag{1}$$

where $[M]$ is the mass matrix of the system, $[C]$ is the damping matrix, $[K]$ the stiffness matrix of the structure and the vector $\{q\} = \{q_1, q_2, \cdots, q_n\}$ is the generalized coordinates vector, where n stands for the number of degrees-of-freedom (DOF) of the model. The load applied along the same generalized coordinated is represented by the vector $\{f(t)\}$ and t stands for the time variable.

2.2. Modal Analysis and Campbell Diagram

Consider the rotating system illustrated in Fig. 1. To analyse the system regarding its modal properties, a null force vector is applied on Equation 1 for free vibrations, with a solution of the form described in the following equation:

$$\{q(t)\} = \{Q(\omega)\}e^{st} = \{Q(\omega)\}e^{(i\omega+\sigma_d)t} \tag{2}$$

where $\{Q\}$ is the amplitude vector of the generalized coordinates and $s = i\omega + \sigma_d$ represents the complex eigenvalues, with σ_d as the decay rate (which is considered null as explained in [14]) and ω the natural frequency. The resulting expression is obtained:

$$(s^2[M(\Omega)] + s[C(\Omega)] + [K(\Omega)])\{q(t)\} = 0 \tag{3}$$

In order to obtain the eigenfrequencies ω, one uses a polynomial eigenvalue solver named $polyeig$ in $Matlab$ [15]. To compute the Campbell diagram, the eigenfrequencies ω are plotted against the rotation speed Ω. A critical speed is determined when the eigenfrequencies match with a spin speed.

2.3. Harmonic Response

On the frequency domain, the force function is assumed to be harmonic, taking the following form:

$$\{f(t)\} = \{F\}e^{i\omega t} \tag{4}$$

Substituting Equations 2 and 4 in the equation of motion 1, the system takes the simple form:

$$(-\omega_{ap}^2\,[M(\Omega)] + i\omega_{ap}[C(\Omega)] + [K(\Omega)])\{Q(\omega_{ap})\}e^{i\omega_{ap}t} = \{F(\omega_{ap})\}e^{i\omega_{ap}t} \tag{5}$$

where ω_{ap} is the applied excitation frequency. For the case of a mass unbalanced, it is modelled as a punctual mass m_u situated at a given distance d from the geometric center of the shaft at an angular position α with respect to the Z axis. The resultant mass unbalance force vector $\{F(\omega)\}$ in the frequency domain, and converted to the complex plane, is given by:

$$\begin{bmatrix} F_u \\ F_w \end{bmatrix} = \Omega^2 m_u d \left[\begin{Bmatrix} sin(\alpha) \\ cos(\alpha) \end{Bmatrix} + j \begin{Bmatrix} -cos(\alpha) \\ sin(\alpha) \end{Bmatrix} \right] \tag{6}$$

where, F_u and F_w represent the frequency domain force amplitudes (in the X and Z directions, respectively), resulting in a synchronous harmonic force with u and w amplitudes growing with the square of the spin speed.

3. METHODOLOGIES

The equipment under analysis in this thesis are a steel beam and the rotor system SpectraQuest's Machinery Fault Simulator (MFS). A model of a steel beam was developed priori to the rotor model and the data acquired with the finite element model (first three natural frequencies) was compared with the

results of the experimental model in order to evaluate the proper functioning of the lab equipment and to gain some experience in experimental modal analysis.

3.1. Analytical Methodology

The analytical solution implemented in this work uses the Rayleigh-Ritz method described in [5]. Considering the undamped asymmetric rotor illustrated in Figure 1 and applying the kinetic energy, strain energy and virtual work equations of the rotor components in Lagrange Equation, the equation of motion becomes:

$$\begin{bmatrix} m & 0 \\ 0 & m \end{bmatrix}\begin{bmatrix} \ddot{q}_1 \\ \ddot{q}_2 \end{bmatrix} + \Omega \begin{bmatrix} 0 & -a \\ a & 0 \end{bmatrix}\begin{bmatrix} \dot{q}_1 \\ \dot{q}_2 \end{bmatrix} + \begin{bmatrix} k_{11} & 0 \\ 0 & k_{22} \end{bmatrix}\begin{bmatrix} q_1 \\ q_2 \end{bmatrix} = \begin{bmatrix} F_{q1} \\ F_{q2} \end{bmatrix} \tag{7}$$

where m stands for the system's mass, a represents the gyroscopic effect, $k_{11} = k + f(l_2)^2 k_{xx}$ and $k_{22} = k + f(l_2)^2 k_{zz}$ are the sum of the system stiffness with the bearing stiffness, with $f(y) = \sin\frac{\pi y}{L}$ as the implemented shape function. Assuming free undamped motion, using a solution in the form of $q_i = Q_i e^{rt}$ (with $r_i = \pm j\omega_i$) and substituting it in Equation 7, it gives the following eigenvalue problem:

$$\begin{bmatrix} k_{11} + mr^2 & 0 \\ 0 & k_{22} + mr^2 \end{bmatrix}\begin{bmatrix} Q_1 \\ Q_2 \end{bmatrix} = 0 \tag{8}$$

Since one is interested in the non-trivial solution of 8, the coefficients Q_1 and Q_2 are selected so that the determinant is zero, i.e.

$$m^2 r^4 + \left((k_{11} + k_{22})m + a^2\Omega^2\right)r^2 + k_{11}k_{22} = 0 \tag{9}$$

To obtain the roots r_1 and r_2 and the respective eigenfrequencies ω_1 and ω_2, one uses a polynomial eigenvalue solver (e.g. $polyeig$ in $Matlab$ [15]). These results yield to the equations that are used to obtain the Campbell diagram.

To study the response to forces due to mass unbalances, one starts to describe the effect of a punctual mass m_u at a distance d from the center of the disk by rewriting the force vector (considering an angular position $\alpha_u = 0$),

$$\begin{bmatrix} F_{q1} \\ F_{q2} \end{bmatrix} = \begin{bmatrix} m_u d f(l_1)\Omega^2 \sin(\Omega t) \\ m_u d f(l_1)\Omega^2 \cos(\Omega t) \end{bmatrix} \tag{10}$$

Substituting Equation 10 in 7 and solving in terms of Q_1 and Q_2, it yields

$$\begin{cases} Q_1 = \dfrac{m_u f(l_1)\Omega^2 d(k_{22} - (m+a)\Omega^2)}{(k_1 - m\Omega^2)(k_2 - m\Omega^2) - a^2\Omega^2} \\ Q_2 = \dfrac{m_u f(l_1)\Omega^2 d(k_{11} - (m+a)\Omega^2)}{(k_1 - m\Omega^2)(k_2 - m\Omega^2) - a^2\Omega^2} \end{cases} \tag{11}$$

The results from the system of Equations 11 are used to obtain the response diagram of the rotor system with the respective bearing conditions. This type of diagram is a plot of the logarithm of the sum of the transversal vibration amplitude $(Q_1 + Q_2)$ against the rotating speed of the rotor's shaft.

3.2. Numerical Models

In this work, the formulation of the finite element models (in $ANSYS$ environment) is based on the following assumptions: the materials are isotropic, homogeneous and presents a linear elastic behaviour; the displacements and deflections of the elements are small when compared to the characteristic dimensions of the structure. The physical properties required to define the material of both models are the Young's modulus $E\ (GPa)$, the Poisson's coefficient ν and the density $\rho\ (kg/m^3)$.

The steel beam was modelled using the BEAM188 finite element (Timoshenko beam theory), with a rectangular cross-section. The model was created using 2 keypoints linked by a line with length $l\ (m)$ and the respective mesh is applied using 50 finite elements per line. Since the beam experimental model is suspended by two nylon strings, the model was computed using free-free boundary conditions at both

ends and an unitary harmonic force $F = 1\,(N)$ is applied in the second keypoint in the Y direction, Figure 2 a), for the harmonic analysis.

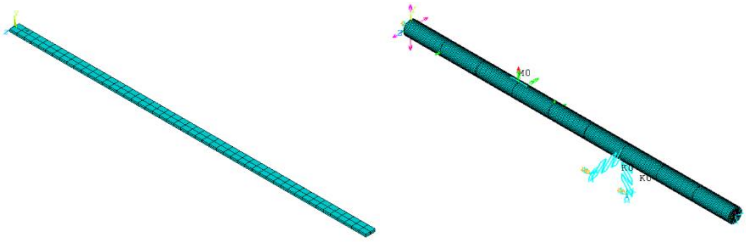

a) b)

Figure 2 – Finite element models used in $ANSYS$: a) Steel Beam; b) Monorotor.

As already mentioned, rotor systems are characterized by a set of basic components, the disk, the shaft, the bearings and a mass unbalanced.

The finite element used to model the aluminum shaft was again the BEAM188 (based on the Timoshenko theory) with a circular cross-section. The shaft model, Figure 2b), was computed using 2 keypoints connected by a line with length $L\,(m)$. Several meshes were developed for different number of finite elements used to characterize the shaft until ensured convergence for first natural frequency. Since the shaft is considered simply supported, fixed-fixed boundary conditions were implemented in all directions (X, Y and Z axis) at both ends.

The rigid disk is represented by the MASS21 finite element (from $ANSYS$), which has up to six dofs. In order to simulate an undamped asymmetric rotor, one implements two spring-damper elements, denominated COMBIN14 (also from $ANSYS$). To simulate an excitation through a mass unbalance (harmonic analysis), two vector forces were computed at the disk position in the X and Z directions. Finally, to prepare the Campbell diagrams, the CAMPBELL command is used in the input file. The PLCAMP command plots Campbell diagram data and the PRCAMP command prints the Campbell diagram data.

3.3. Experimental Models

In this section, the procedures and models used for each experimental test are introduced. A experimental modal analysis is performed to a rectangular cross-section beam, and its results are compared with the numerical solution. The beam's response was calculated under free body conditions, therefore it was suspended on a portal crane using two nylon strings (Figure 3a)). An impact hammer equipped with a rubber tip generates the excitation signal and the dynamic response of the structure is measured by an accelerometer attached to the beam using bee wax. The signal is treated and saved for posterior processing and analysis.

a) b)

Figure 3 – Experimental models: a) Steel Beam suspended on a portal crane; b) SpectraQuest's Machinery Fault Simulator (MFS) used for resonance test.

As already mentioned, the rotor system used to conduct the modal tests for this thesis was the SpectraQuest's Machinery Fault Simulator (MFS), illustrated in Figure 3 b). The experiment was divided in two stages in order to achieve the following objectives: determine the rotor natural frequencies at rest; obtain the rotor critical speeds.

The first stage was accomplished by performing the impact hammer test on the rotor system at rest. The test was carried out for three different locations, the shaft, the disk and the bearings. For each of these locations, measurements were made in X and Z directions (D_X, D_z, S_X , S_Z, B_X and B_Z) by mounting the accelerometer in the horizontal and vertical directions respectively in order to determine the natural frequencies at rest in both directions, as illustrated in Figure 4a). In the second stage, one computes the Autospectrum of the rotor machinery in operation to acquire the system critical speeds. Measurements were taken for four different rotation speeds (5 Hz, 10 Hz, 20 Hz and 30 Hz). Considering that the rotor must in motion throughout the procedure, the accelerometer was positioned in the bearings horizontally, as shown in Figure 4 b). In addition, a Stroboscope was used to witness the BW and FW motion (described with more detail in the main document [14]).

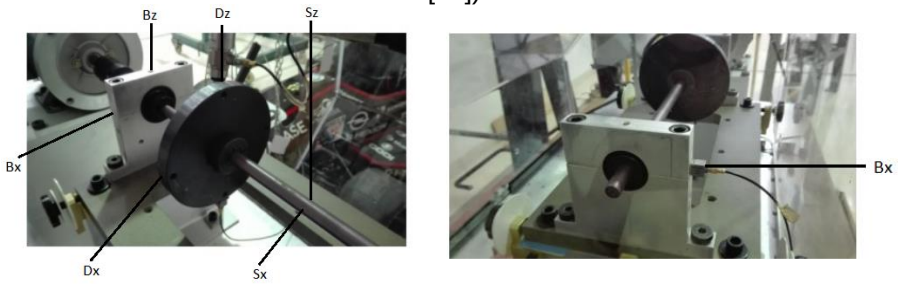

a) b)

. Figure 4 – Accelerometer mounting positions: a) First stage; b) Second stage.

4. Results and Discussion

This chapter consists on the presentation and discussion of the analytical, numerical and experimental results obtained throughout this work.

4.1. The Model

In this thesis, all three rotor models are based on the one introduced by Lalanne and Ferraris [5], illustrated in Figure 5. The rotor is composed by a shaft of length $L = 0{,}34\ m$, radius $R_1 = 0{,}0065\ m$, material density $\rho_S = 2712\ kg/m^3$ and Young's Modulus $E_S = 69 \times 10^9 Pa$. The rigid disk located at $Y = l_1$ has a radius $R_2 = 0{,}066\ m$, thickness $h = 0{,}016\ m$, material density $\rho_D = 7850\ kg/m^3$ and Young's Modulus $E_D = 200 \times 10^9 Pa$. A discrete bearing is located at $= l_2$. In this article, one considers an undamped asymmetric rotor.

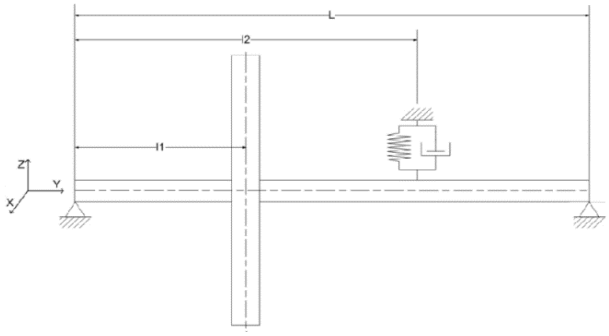

. Figure 5 – Model of the mono-rotor (source [8]).

The rotor model consists of fifteen Euler-Bernoulli beam elements, with sixteen nodes. Taking this into account, the boundary conditions are to be applied at nodes 1 and 16 of the shaft, the disk and mass unbalanced forces at node 6 and finally the bearing at node 12.

4.2. Verification: Numerical $versus$ Analytical Model

In this section, one compares the results obtain with the FEM and the Rayleigh-Ritz method, considering only the case of an asymmetric rotor (the main document includes the study of a symmetric rotor, as well). In addition, each case is carried out for two hypothesis, one where the disk is located in the middle of the shaft ($l_1 = L/2$) and a second where the disk is positioned at $l_1 = L/3$.

Considering the undamped asymmetric rotor ($k_{xx} = 2{,}3 \times 10^4\ N/m$ and $k_{zz} = 1{,}27 \times 10^5 N/m$) of Figure 5. To determine the analytical solution one applied the methodology presented in section 3.1 to plot the Campbell diagram. Having the rotors mass $[M]$, damping $[C]$ and stiffness $[K]$ matrices (Equation 7), they are introduced in a polynomial eigenvalue solver (e.g. $polyeig$ in $Matlab$), which is used to obtain the roots $r_i = \pm j\omega_i$ of the characteristic equation 9 and the respective eigenfrequencies ω_i , for the interval $\Omega = [0{,}9000][rpm]$.

For the FEM, one used the methodology described in section 2.2 to obtain the Campbell diagram, in $Matlab$, of the undamped asymmetric rotor finite element model illustrated in Figure 5. For the $ANSYS$ model, one applies the methodology presented in section 3.2, the eigenfrequencies are determined using the QRDAMP command in the input file, while the plot of the Campbell diagram is performed using the PLCAMP command and the PRCAMP command prints the Campbell diagram data. Figures 6 a) and b) illustrate the Campbell diagrams for the Rayleigh-Ritz method and the FEM considering the first hypothesis (disk positioned at $l_1 = L/2$) and the second hypothesis (disk positioned at $l_1 = L/3$).

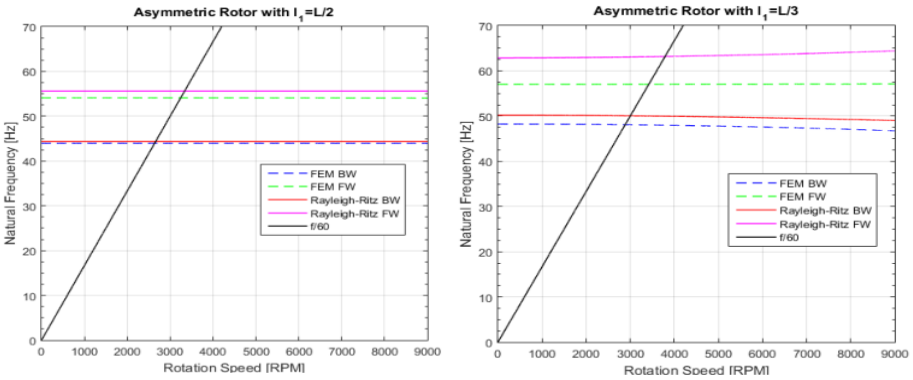

Figure 6 – Campbell Diagram of the asymmetric rotor: a) Disk position $l_1 = L/2$; b) Disk position $l_1 = L/3$.

Table 1 shows the natural frequencies and critical speeds taken from the Campbell diagrams for the three models, considering both disk positions.

Table 1 – Asymmetric rotor first and second natural frequency and critical speeds for both disk positions.

Method	Frequency at Rest (Hz)				Critical Speeds (rpm)			
	$l_1 = L/2$		$l_1 = L/3$		$l_1 = L/2$		$l_1 = L/3$	
	BW	FW	BW	FW	BW	FW	BW	FW
Rayleigh-Ritz	44,38	55,59	50,19	62,87	2663	3335	3003	3790
Matlab	43,93	54,11	48,22	57,03	2636	3246	2884	3423
ANSYS	44,26	54,92	48,32	57,17	2655	3294	2890	3431

Observing the results, one may conclude that for a disk position at $l_1 = L/2$, the frequency difference at rest and the critical speeds difference between the FEM and the Rayleigh-Ritz method are very low. However, for $l_1 = L/3$ the differences become more noticeable. The frequencies at rest and critical speeds obtained with the FEM are lower when comparing with the computed solution using the Rayleigh-Ritz method, which can be explained analysing the first mode shape. In the Rayleigh-Ritz method, the shape function, $f(y) = \sin(\frac{\pi y}{L})$, is considered for the exact solution of a beam's first vibration mode, which presents a maximum value of $f(y) = 1$ for $y = L/2$ and a minimum value of $f(y) = 0$ for $y = L$, implicating that the shape function does not take into account the effect of the concentrated mass (disk) located at $Y = l_1 = L/3$. Thus, one may anticipate better results from the FEM since the model's computed deformation has a better adjustment to the real deformation.

Additionally, an harmonic analysis is performed for a disk's location $l_1 = L/3$. For the analytical solution, one uses the methodology described in section 3.1, which states that a mass unbalanced applied in a rigid disk results in a synchronous harmonic force (Equation 10). As for the FEM, one used the methodology presented in section 2.3, the same mass unbalanced is applied to node six of the undamped asymmetric rotor of Figure 5. Subsequently, the response amplitudes for displacements u, w (in the X and Z directions, respectively) are obtained for the finite element model using Equation 5.

The Response diagrams of the asymmetric rotor for the FEM and Rayleigh-Ritz method are shown in Figures 7 a) and b).

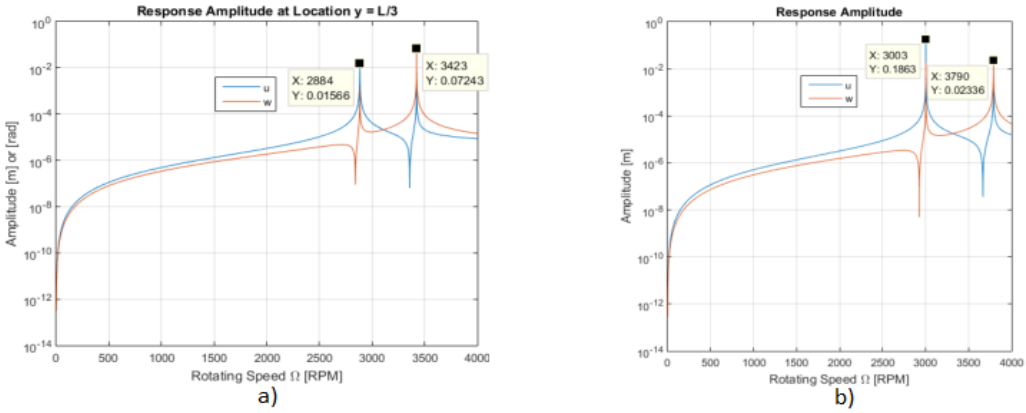

Figure 7 – Response diagram asymmetric rotor ($l_1 = L/3$): a) FEM; b) Rayleigh-Ritz.

Observing the graphics of Figures 7 a) and b), it clearly illustrates two maximum amplitudes located at the same system's critical speeds for each respective model (u is maximum in the first critical speed and w is higher in the second critical speed), as shown in Table 1. During the subcritical range one observes that the response amplitude u (in X direction) presents a higher value than w (in the Z direction). This can be justified by the fact that the bearing stiffness in the Z direction is higher than the one added in the X direction, $k_{zz} > k_{xx}$.

4.3. Validation: Numerical *versus* Experimental Model

Before analysing the rotor experimental model, one started by comparing the beam's results extracted by the numerical model with the data obtained with the experimental test. To determine the numerical solution, one used the methodology presented in section 3.2 applied to the beam finite element model illustrated in Figure 2 a), with the following properties: Young's Modulus $E = 185\ GPa$, Poisson's coefficient $\nu = 0{,}3$, mass density $\rho = 7820\ kg/m^3$, length $L = 800mm$, height $h = 21mm$ and width $w = 5.5\ mm$.

For the experimental test, one applied the methodology described in section 3.3 to the steel beam, illustrated in Figure 3 a), with the same mechanical properties as the ones used in the numerical model. The specimen was suspended on a portal crane using two nylon strings, to simulate free body conditions. The uni-axial accelerometer was attached to the beam using bee wax and an impact hammer equipped with a rubber tip was used to excite the structure. Figure 8 a) presents the FRFs computed from the steel beam experimental and numerical models.

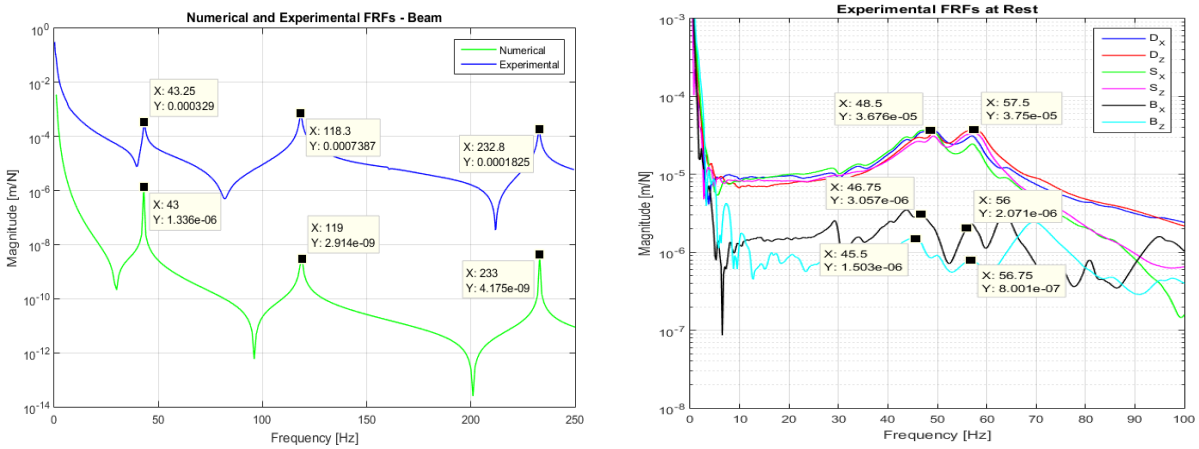

Figure 8 – Frequency response functions: a) Steel beam; b) Disk, shaft and bearings on the horizontal and vertical directions.

Analysing the graphic from Figure 8 a), it is easy to identify the models first, second and third natural frequencies of the steel beam (43 Hz, 118 Hz and 233 Hz). Thus, one may confirm that the numerical model is well adjusted to the experimental model in terms of the natural frequencies, completing the objectives established for this particular test. Also, the difference in amplitude may be explained by the different forces applied (in FEM, $F = 1$). At this point, one has verified the proper functioning of the lab equipment in order to proceed to the model test in the MFS.

The next step involves the comparison of the results obtained in section 4.2, with the experimental data collected using the methodology (first and second stage) presented in section 3.3 for the MFS.

The experimental test performed in the first stage follows the methodology described in section 3.3 applied to the experimental rotor system at rest. Figure 8 b) shows measurements of the rotor's response performed for the six pre-established accelerometer positions, as illustrated in Figure 4 a). Observing the graphic, one highlighted some of the peaks that represent the expected first ($\cong 47{,}80\ Hz$) and second ($\cong 57{,}19\ Hz$) natural frequency of the rotor. One notices that, in most cases, the natural frequencies of the experimental model are higher than the numerical models frequencies. Regardless, one may conclude that the natural frequencies acquired by the experimental model are very similar to the ones obtained with both numerical models, contributing to the validation of the numerical models. Having completed the natural frequency study, one proceeds with the analysis of the critical speeds.

For the second stage, one used the methodology described in section 3.3 to the experimental rotor in operation. Figure 9 shows measurements taken considering four operational spin speeds (5 Hz, 10 Hz, 20 Hz and 30 Hz). During the whole procedure, the accelerometer was positioned horizontally on the bearing (B_X), as illustrated in Figure 4 a).

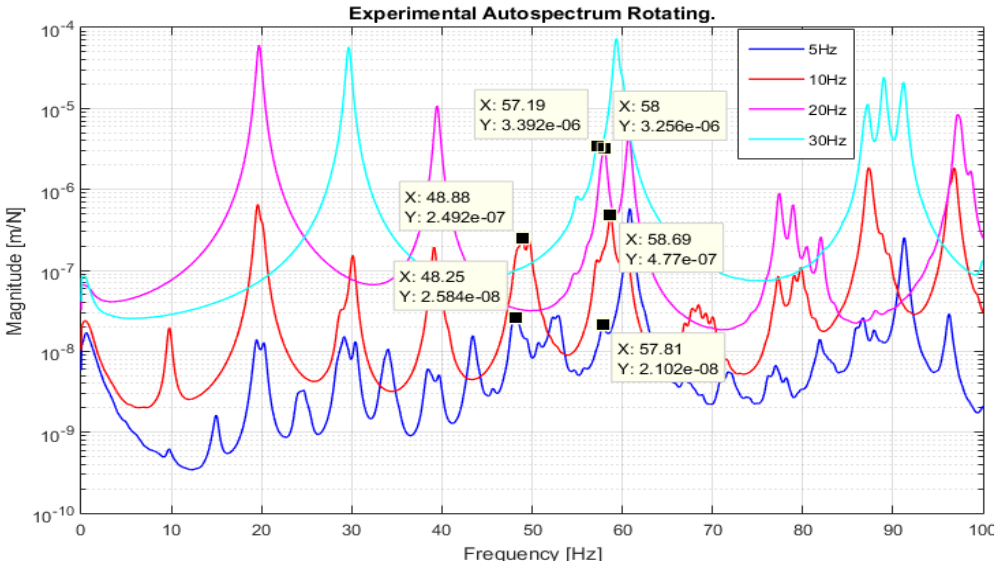

Figure 9 – Experimental Autospectrum of the MFS at position B_X, considering a rotation speed of 5 Hz (300 RPM), 10 Hz (600 RPM), 20 Hz (1200 RPM) and 30 Hz (1800 RPM)

Examining the graphic, one notices that each curve indicates a clear maximum at the rotor's rotating frequency and their respective multiples. For example, the Autospectrum that corresponds to a spin speed of 20 Hz presents a peak exactly at that frequency and (with a lower intensity) at higher multiples (40 Hz, 60 Hz...), but these are not the frequencies of interest. As a result, one decided to mark the peaks that represent the expected first and second critical speeds values, as shown in Figure 9.

Additionally, one notices that the first critical speed was not detected by the autospectrum curves that correspond to a shaft spin speed of 20 Hz and 30 Hz, implying that BW peaks are usually not observed in practice. Nevertheless, good accuracy is obtained, at least for the first two critical speeds ($\cong 48{,}57\ Hz$ and $\cong 57{,}98\ Hz$, respectively), without considering "foundation" effects. Comparing with results displayed in Table 1, one concludes that the critical speeds obtained with the experimental model are very close to the ones acquired with both numerical models. Thus, the combination of the results achieved in the first and the second stage offer the validation of the numerical methodology (FEM), completing the main objective of this thesis.

After acquiring the validation of the numerical method, one implemented the FEM to the Propfan Engine, as shown in the main document [14].

5. Conclusions

Encouraged by the need for more convenient and efficient means to analyse the dynamic behaviour of rotation machinery, this thesis main objective has been to validate a numerical method (FEM) to study the vibrational response of a rotor system. In order to achieve this, one compared the natural frequencies and critical velocities obtained by the MFS equipment with the results from the numerical models, thus validating the numerical methodology used in this work.

Satisfying results were easily obtained for the steel beam analysis, since the first three frequency differences between the numerical and experimental models were very, approving the well functioning of the lab equipment and providing valuable experience in modal testing. The FRFs obtained from the impact hammer test carried out for the MFS (first stage) revealed distinctive peaks at approximately 47,8 and 57,19 Hz, which correspond to the rotor's first and second natural frequency respectively. These values proved to be quite similar with the data acquired from both numerical models ($Matlab$ and $ANSYS$) shown in Table 1. As for the second stage, one also found a coherence between the critical speeds obtained with the numerical model and the values observed in the autospectrum curves (Figure 9). Despite the fact that for high shaft spin speeds the dampening effect becomes too high to observe the intended results, for lower rotating speeds the critical speed values are visible and similar with the ones acquired using the FEM.

Acknowledgment

I would like to express my sincere gratitude to Professor Miguel Matos Neves from DEM, IST, for the opportunity of working with him and for the patience, support and guidance throughout the development of this work. I must also leave a word of gratitude to Professor Hugo Policarpo for his constant availability and suggestions concerning the experimental tests performed in the laboratory.

References

[1] R. Ruhl and J. Booker. A finite element model for distributed parameter turborotor systems. *Journal of Engineering for Industry*, 1972.

[2] H. Nelson and J. McVaugh. The dynamics of rotor-bearing systems using finite elements. *Journal of Engineering for Industry*, 1976.

[3] H. Nelson. A finite rotating shaft element using Timoshenko beam theory. *Journal of Mechanical Design*, 1980.

[4] G. Genta. Consistent matrices in rotor dynamics. *Meccanica*, 1985.

[5] M. Lalanne and G. Ferraris. *Rotordynamics Prediction in Engineering*. Chhichest: Wiley and Sons, 2nd edition, 1998.

[6] G. Genta. *Dynamics of Rotating Systems*. New York: Springer, 1998.

[7] J. Rao. *History of Rotating Machinery Dynamics*. Springer Netherlands, 2011.

[8] R. Carvalho. A frequency-domain methodology for rotordynamics: Analysis and force identification. Master's thesis, Instituto Superior Técnico, Lisboa, Portugal, 2012.

[9] M. Matos. Balancing and force identification in rotordynamics. Master's thesis, Instituto Superior Técnico, Lisboa, Portugal, 2013.

[10] C. W. de Silva. *Vibration and Shock Handbook (Mechanical Engineering)*. CRC Press, 2005.

[11]Maia, Silva, He, Lieven, Lin, Skingle, To and Urgueira. *Theoretical and experimental modal analysis*. Research Studies Press, 1998.

[12] B. Schwarz and M. Richardson. Experimental modal analysis. *Vibrant Technology, Inc*., 1999

[13] H.H. Jeffcott. The lateral vibration of loaded shafts in the neighbourhood of a whirling speed – The effect of want of balance. *Philos*. *Mag*, 1919.

[14] L. Franco. Frequency domain response of a propfan using finite element method and experimental study on a rotor. Master's thesis, Instituto Superior Técnico, Lisboa, Portugal, 2017.

[15] MathWorks. Matlab documentation, 2013. URL http://www.mathworks.com/help/matlab/index.html.